Carbon adsorption on and diffusion through the Fe(110) surface and in bulk: Developing a new strategy for the use of empirical potentials in complex material set-ups

Iwan Halim Sahputra[1], **Aurab Chakrabarty**[1], **Oscar Restrepo**[1,2], **Othmane Bouhali**[1], **Normand Mousseau**[2], **Charlotte S. Becquart**[3], and **Fedwa El-Mellouhi**[*,4]

[1] Science Program, Texas A&M University at Qatar, Doha, Qatar
[2] Département de Physique, Université de Montréal, Canada
[3] UMET, UMR 8207, Ecole Nationale Supérieure de Chimie de Lille, Université Lille I, France
[4] Qatar Environment and Energy Research Institute, Hamad Bin Khalifa University, Doha, Qatar

* Corresponding author: e-mail felmellouhi@qf.org.qa, Phone: +974 4454 7284, Fax: +974 4454 0281

Oil and gas infrastructures are submitted to extreme conditions and off-shore rigs and petrochemical installations require expensive high-quality materials to limit damaging failures. Yet, due to a lack of microscopic understanding, most of these materials are developed and selected based on empirical evidence leading to over-qualified infrastructures. Computational efforts are necessary, therefore, to identify the link between atomistic and macroscopic scales and support the development of better targeted materials for this and other energy industry. As a first step towards understanding carburization and metal dusting, we assess the capabilities of an embedded atom method (EAM) empirical force field as well as those of a ReaxFF force field using two different parameter sets to describe carbon diffusion at the surface of Fe, comparing the adsorption and diffusion of carbon into the 110 surface and in bulk of α-iron with equivalent results produced by density functional theory (DFT). The EAM potential has been previously used successfully for bulk Fe–C systems. Our study indicates that preference for C adsorption site, the surface to subsurface diffusion of C atoms and their migration paths over the 110 surface are in good agreement with DFT. The ReaxFF potential is more suited for simulating the hydrocarbon reaction at the surface while the subsequent diffusion to subsurface and bulk is better captured with the EAM potential. This result opens the door to a new approach for using empirical potentials in the study of complex material set-ups.

© 2016 WILEY-VCH Verlag GmbH & Co. KGaA, Weinheim

1 Introduction Carburization of a metal surface is a phenomenon frequently observed for iron and its alloys exposed to hydrocarbon atmosphere at elevated temperature. Catalytic reactions with hydrocarbons lead to adsorption of atomic carbon into metal surface that diffuses to subsurface and forms carbides. These reactions can produce a number of undesirable outcomes such as production of coke − that impairs heat transfer efficiency, reduction of metal catalyst lifetime, and eventually catastrophic failure of structural integrity of the material with potentially costly consequences to industries, particularly in the Oil and Gas sector [1]. Therefore, it is important to understand these processes and to investigate further how to reduce or prevent these material failures. Yet, because they occur in harsh environments and are of kinetic nature, the microscopic mechanisms associated with carburization and metal dusting have been very difficult to identify and most attempts to avoid the problem have followed empirical pathways, producing generally over-cautious and costly solutions.

Formally, computational approaches offer a promising route to unveil the origin of carbon migration and propose

solutions through materials design. A number of technical hurdles must still be addressed, however, before we are able to tackle the full problem. This paper addresses one of the central hurdles that have prevented earlier computational study of this problem: the selection of force field. Indeed, even though quantum mechanical description, through density functional theory, is accurate enough to identify C segregation and carbide formation mechanisms, this approach remains extremely computationally demanding, even with current supercomputers, preventing its application to the full-scale problem. It is, therefore, necessary to resort to empirical potentials that must be fully characterized over the full set of relevant binding environments encountered during the kinetic process.

Here, we assess a few recently-proposed empirical potentials for the Fe/C system, focusing mainly on a proposed force field based on the embedded atom method (EAM) formalism initially developed by Daw and Baskes [2]. This EAM potential was fitted and tested with the goal of investigating the behavior of carbon in Fe [3]. The parameter set was then modified to make the potential landscape around the saddle point more realistic [4]. This Fe–C potential has been widely used to model Fe–C systems, with a particular focus on carbon-dislocation interactions [5–7] and the dynamics of carbon in bulk Fe [3, 8]. It was also used to model internal friction experiments [9], martensite properties [10], and C ordering in Fe–C crystallites at high C concentrations [11]. However, the potential was not specially fitted for a system with carbon on Fe surfaces, furthermore, it cannot be applied to study the reaction between hydrocarbon and Fe surfaces as no interaction is available for hydrogen. As an alternative potential, we consider two parameter sets of the ReaxFF potential [12, 13] based on a parameter set derived by van Duin et al. [14] and specifically designed for catalytic reaction studies of C/H/O–Fe surface systems. This potential, however, was not rigorously fitted for a bulk system. Therefore, the performances of both potentials need to be assessed, and a strategy to utilize them for studying mechanisms from surface to bulk must be found. The primary objective of this paper is to assess both potentials for surface related studies and perform preliminary C-diffusion studies.

In the first part of this study, structural properties are tested by first calculating the elastic constants and free surface energy of α-iron using the various empirical potentials and comparing them to DFT as well as experimental results. We then present carbon adsorption on Fe(110) surface and its absorption in bulk Fe. In the second part, the minimum energy path for carbon diffusion on the Fe(110) surface and in bulk Fe computed with the EAM potential, that presents the best agreement with DFT, are presented and discussed. The suitability of the potentials for reproducing proper carbon diffusion on, into, and in Fe are assessed by comparing calculated properties against experimental measurements and ab initio DFT calculations. Results lead to the suggestion of a combined strategy for the use of empirical potentials for the study of complex set-ups.

2 Computational methods

2.1 DFT calculations DFT calculations were done using the VASP code [15–17]. The projector-augmented wave (PAW) pseudopotential method with PBE exchange-correlation functionals were used. A 13-layer-thick surface supercell with a vacuum of 16 Å was chosen to test the convergence of the layer-wise relaxation of the surface. The first five layers were allowed to relax in all directions while the next three layers were allowed to move only perpendicularly to the surface. The remaining layers were kept frozen to imitate an infinite bulk. It is shown in reference [18] that the structure relaxation for the reconstruction of the surface converges over a depth of less than five layers. This can be seen in Table 3. For the production of nudged elastic band (NEB) results, which are computationally exhaustive, a 4×4 multiple of Fe-110 surface periodic unit cell with seven layers parallel to the surface was chosen, with a vacuum of 16 Å. The pure-Fe supercell has 112 atoms with a surface area of 90 Å^2. For the NEB calculation of the surface-to-subsurface diffusion, eight interpolated images are used, while 12 images are used for the surface migration of carbon. A force tolerance of 0.001 eV Å^{-1} is used for all calculations. A k-point mesh is automatically generated using Monkhorst–Pack grid. For the relaxation calculations, a $7 \times 7 \times 1$ grid is used while we chose a coarser $5 \times 5 \times 1$ grid for the NEB minimum energy path calculations.

2.2 EAM set-up Three different supercell models for the (110) surface have been generated for surface energy calculations. They are described in Table 1. The LAMMPS [19] simulation code was used for all the EAM calculations.

Periodic boundary conditions were applied along all the directions and the total energy of the system was first minimized to relax the bulk. The X-length was then increased to 150 Å to create a vacuum region above the free surface much larger than the potential cutoffs and the total energy was minimized a second time. Figure 1 presents the system. The minimization of energy was done using the conjugate gradient algorithm using 1×10^{-6} eV Å^{-1} stopping tolerances with respect to forces in all directions. Fe atoms at the bottom layers (15 Å length) were frozen in order to mimic bulk Fe by setting zero forces on them.

For carbon adsorption and absorption calculations, we used the 1300-atom supercell (model 1). The simulation box

Table 1 Models for Fe(110) surface energy calculations.

	model 1	model 2	model 3
x-dimension (lattice unit)	13	15	15
y-dimension (lattice unit)	5	5	6
z-dimension (lattice unit)	5	5	6
surface 110 area (Å^2)	288.18	288.18	414.98
number of Fe atoms	1300	1500	2160

Phys. Status Solidi B 254, No. 2 (2017)
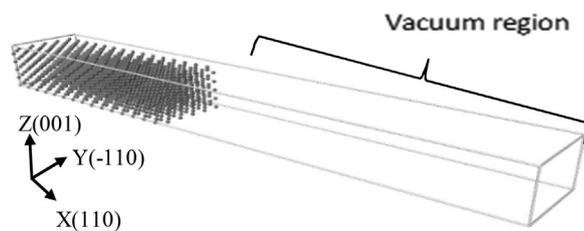
Original

Paper

(3 of 10) 1600408

Figure 1 Visualization of the Fe system with a free surface on the (110) direction, dimension are given in Table 1. Periodic boundary condition is applied to all directions (X, Y, and Z).

dimension was $52.5 \times 20.2 \times 14.3 \, \text{Å}^3$ with periodic boundary conditions along all directions. The X-length was then increased to $150 \, \text{Å}$ to create a vacuum region above the free surface. Fe atoms at the bottom layers ($15 \, \text{Å}$ length) were frozen in order to mimic bulk Fe by setting zero forces on them. A carbon atom was placed on the Fe(110) surface at the different symmetric adsorption sites shown in Fig. 2, and the system was relaxed again. For absorption, carbon was placed in the subsurface.

For carbon in the bulk calculations, a 1300-atom bulk supercell (model 1) was used without creating a free surface. The simulation box dimension was $52.5 \times 20.2 \times 14.3 \, \text{Å}^3$ with periodic boundary conditions along all directions. A carbon atom was then introduced at the octahedral or tetrahedral site and after that relaxed. The minimum energy paths of carbon migration on surface, diffusion into subsurface and in bulk Fe have been calculated using the climbing image nudged elastic band (CI-NEB) method implemented in LAMMPS [20–22]. The damped dynamics method [23] was used for energy minimization in the NEB calculation. An inter-replica spring constant of 1 and a time step of 0.05 ps were used. A force tolerance of $0.001 \, \text{eV} \, \text{Å}^{-1}$ was applied for the energy minimization during NEB calculations with 16 replicas.

2.3 ReaxFF set-up The same set up as for EAM was used for the ReaxFF potentials [12, 13]. The properties of interest are Fe surface and bulk properties, carbon adsorption, absorption, and in Fe bulk properties. The LAMMPS [19] simulation code was used for all the ReaxFF calculations. ReaxFF-1 refers to calculations done with the
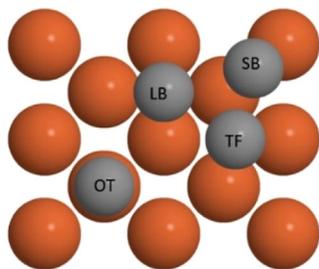

Figure 2 Initial carbon position on the Fe(110) surface: short bridge (SB), threefold (TF), long bridge (LB), on top (OT). Grey: carbon atom, brown: Fe atoms.

potential derived in [12] whereas ReaxFF-2 refers to calculations done with a revised version of the potential with optimized Fe–Fe bonds upon C-insertion, published in [13]. For the ease of representation, none of the ReaxFF versions is explicitly mentioned when a feature common to both of the versions is presented.

2.4 k-ART simulations Simulations with the kinetic activation–relaxation technique (k-ART) were done using the same 1300-atom system (model 1) with a carbon atom initially placed in the bulk. The carbon atom was allowed to diffuse through the bulk and to find its path to the surface, jumping between minimum energy configurations by crossing energy barriers.

K-ART [24], an off-lattice kinetic Monte-Carlo algorithm with on-the-fly catalog building, is briefly described here. At every step, the local environment, described by its topology, is assessed. If all environments are known, events are imported from the catalog, if not, new searches are made using the open-ended activation–relaxation technique (ART nouveau) [25–27], with the force provided by the LAMMPS library. Each set of initial, barrier and final minimum configurations is counted as a possible event and is added to the catalog using a topological classification [28, 29]. At every step, the most probable events (with a probability of occurrence of 1 in 10000 or more) are fully reconstructed and the energy barrier reconverged to take into account all elastic and structural deformations. The clock is then brought forward according to the KMC algorithm [30, 31] and an event is selected with a weight proportional to its rate defined as $r_i = \left(10^{13} \text{s}^{-1}\right) e^{E_m/k_B T}$ were E_m is the migration energy and $T = 600 \, \text{K}$ is the temperature. $600 \, \text{K}$ was chosen because the technically relevant phenomena, such as carburisation and metal dusting, are often observed around this temperature. [32, 33]. A more detailed description of the algorithm and applications to alloys and disordered systems can be found in [34, 35].

2.5 Details of analysis Surface energies (E_s) are calculated using the following equation:

$$E_s = [E_{total}(\text{free}) - E_{total}(\text{bulk})]/2A, \tag{1}$$

where $E_{total}(\text{free})$ and $E_{total}(\text{bulk})$ are the total energies of the system with the free surface and the bulk system respectively and A is the cross-sectional area of the system with the free surface. The surface reconstruction parameter (δz) is the change in the interlayer spacing as a percentage of the interlayer spacing of the bulk system.

$$\delta z_n = \frac{z_n - z_0}{z_0} \times 100, \tag{2}$$

where z_n is the separation of the n-th layer (the surface layer being the 1st) from the next layer and z_0 is the layer separation in bulk.

The adsorption energy is usually calculated using the following equation:

$$\Delta E = E(\text{Fe}_n\text{C}) - E(\text{Fe}_n) - E(\text{C}), \qquad (3)$$

where $E(\text{Fe}_n\text{C})$ is the potential energy of the Fe(110) system containing a carbon atom, $E(\text{Fe}_n)$ is the potential energy of the bulk Fe system, and $E(\text{C})$ is the energy of an isolated C atom. However, in practice, the C atom always gets adsorbed in metal through hydrocarbon-metal reactions and taking the energy of an isolated C atom does not represent a physically sound estimate of adsorption energy. Furthermore, the energy of an isolated C atom cannot be computed with LAMMPS. Therefore, the energy difference with the most stable configuration is a more appropriate value to be determined.

The shear modulus, C', is calculated using the following equation:

$$C' = (C_{11} - C_{12})/2, \qquad (4)$$

and the bulk modulus, B, from

$$B = (C_{11} + 2C_{12})/3, \qquad (5)$$

where C_{11} and C_{12} are elastic constants.

3 Assessment of the empirical potentials

3.1 Bulk properties of α-Fe
The DFT-PBE calculation predicts a lattice parameter for bulk Fe of 2.83 Å, close to the experimental value (extrapolated to 0 K) of 2.86 Å [36], while the EAM prediction is 2.85 Å. The EAM predicts a 4.013 eV cohesive energy which is lower than the experimental data of 4.27 eV [37]. The vacancy formation energy predicted by the EAM is 1.71 eV which is lower than the DFT calculations which range from 1.95 to 2.25 eV [38, 39] but higher than the experimental data of 1.4 eV [40]. According to the ReaxFF potential calculations, the cohesive energy of Fe is 4.31 eV and the vacancy formation energy is 2.49 eV.

To calculate the elastic constants of bcc-Fe, small strains were applied to the bcc-Fe system with equilibrium lattice parameter using the script for computing elastic constant included in the LAMMPS package. Changes in stress and strains were used to compute the three non-identical elastic constants C_{11}, C_{12}, and C_{44}. The calculated

elastic constants, together with the shear modulus and bulk modulus are presented in Table 2.

The elastic constants predicted by the EAM are close to the experimental data [41]. Note that the Fe potential comes from reference [42], and therefore, the results we obtained for the elastic constants are identical to those in reference [42]. ReaxFF-1 predicts one constant, C_{11}, in excellent agreement with the experimental data and the other elastic constants within 10% of the experimental value, except for C', which is overestimated by about 20%. While the discrepancy is slightly larger than for EAM, these values are overall in good agreement with experiment.

3.2 Fe surface properties
Table 3 presents the (110) surface energy (E_s) and surface reconstruction parameter (δz_n) calculated using the EAM, the ReaxFF-1, and DFT. ReaxFF-2 results for these parameters are very close to these values and are not explicitly given. A comparison to experimental data are also presented. The differences in atom number and surface area do not induce significant differences of the surface relaxation properties. The EAM predicts a lower surface energy than that estimated by DFT calculations and experiment while the ReaxFF potentials predicts a surface energy close to the DFT calculation and experiment. Note, however, that the experimental data were obtained using liquid surface tension measurements and extrapolation of the data to 0 K. Both potentials predict a contraction of the first layer (δz_1) which is not consistent with DFT calculations and experiments. However, due to the large uncertainty in the experimental measurements as shown in Table 3, the values are still within the experimental ranges (1 ± 2 and 0.5 ± 2). For the second layer (δz_2), the EAM predicts an expansion, which is in agreement with the DFT calculation and experiment while ReaxFF predicts a contraction. However, again due to the large uncertainty in the experimental measurements, the ReaxFF's value is still within the experimental range. For the three other layers, EAM predicts expansions while ReaxFF predicts contractions. These values are not consistent with the DFT calculations. However, as the magnitude of the relaxations is very small, this discrepancy might not be significant.

3.3 Carbon adsorption and absorption
Carburization of the iron surface commonly occurs by reaction with hydrocarbons. As the end result of these reactions, carbon is

Table 2 Elastic constants of bulk Fe. The experimental data is extrapolated from 3 to 0 K.

elastic constant (GPa)	expt. [41]	EAM [42]	EAM		ReaxFF-1	
			1% strain	0.1% strain	1% strain	0.1% strain
C_{11}	239.55	243	243.27	243.34	239.85	239.92
C'	51.90	49	49.09	49.14	62.67	62.72
C_{44}	120.75	116	116.12	116.14	114.48	114.49
B	170.35	177.7	177.82	177.81	156.29	156.30

Original

Paper

Phys. Status Solidi B 254, No. 2 (2017)   (5 of 10) 1600408

Table 3 Surface energy and relaxation parameters for the Fe(110) surface.

	E_s (J m^{-2})	δz_1 (%)	δz_2 (%)	δz_3 (%)	δz_4 (%)	δz_5 (%)
EAM						
model 1	1.617	−0.220	0.018	0.018	0.019	0.019
model 2	1.617	−0.220	0.018	0.018	0.018	0.020
model 3	1.617	−0.220	0.018	0.018	0.018	0.020
ReaxFF-1						
model 1	2.182	−0.135	−0.283	−0.303	−0.305	−0.302
model 2	2.181	−0.134	−0.285	−0.302	−0.301	−0.307
model 3	2.181	−0.135	−0.284	−0.302	−0.302	−0.307
DFT	2.44	0.04	0.11	−0.22	−0.08	0.03
expt. (surf. tension) [43]	2.41	–	–	–	–	–
expt. (MEIS) [44]	–	1 ± 2	0.5 ± 2	–	–	–
expt. (LEED) [45]	–	0.5 ± 2	–	–	–	–

adsorbed on the iron surface and then diffuses further into the subsurface [1]. This section investigates how carbon is adsorbed on the Fe(110) surface, by testing various possible locations of carbon on the Fe(110) surface to find the lowest energy site for carbon adsorption. Then carbon absorption in the subsurface is considered.

3.3.1 Carbon adsorption on surface When adsorbed on the Fe(110) surface, carbon prefers to be on a LB site according to all empirical potential calculations, in agreement with our DFT calculations as well as those of others [46]. In all empirical potential calculations, the carbon remains at its original location for the long bridge (LB), and on-top (OT) sites after energy minimization. The EAM predicts that a carbon initially located at a short bridge (SB) site moves to a threefold (TF) site after energy minimization. With ReaxFF, a carbon initially located at SB and TF sites moves to a LB site after energy minimization. Therefore, in order to calculate the adsorption energy at SB and TF sites, the carbon has to be frozen at these positions during energy minimization. Figure 3 shows the most stable structure of carbon on the Fe(110) surface, where the carbon atom, for all empirical potentials is located on LB site. The EAM places the carbon atom at a slightly higher position above the surface than where the ReaxFF puts it.
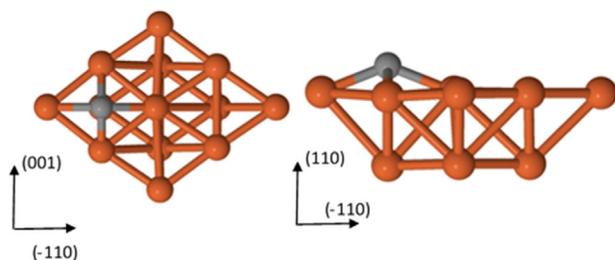

Figure 3 Most stable structure (LB) of carbon on a Fe(110) surface calculated using the EAM and the ReaxFF, where the EAM puts the carbon at a slightly higher position than the ReaxFF or DFT. Brown: Fe atoms, grey: carbon atom. Only surface with (4 × 4) cells are shown.

Table 4 shows the adsorption energies relative to the most stable configuration (LB site). Both potentials predict the OT site as the most unstable configuration and the EAM predicts an OT relative adsorption energy close to the DFT calculation.

3.3.2 Carbon absorption in the subsurface EAM predicts that the carbon atom prefers to be at an octahedral site in the Fe subsurface, in agreement with this work DFT calculations and literature [46]. According to the EAM potential, in this configuration, one Fe atom is slightly pushed away from the surface as shown in Fig. 4A. Furthermore, when the carbon atom is introduced in a tetrahedral site in the subsurface, it moves to the surface after energy minimization, which is in agreement with the DFT calculations. On the other hand, according to the ReaxFF calculations, the preferred position for carbon in the subsurface is not the octahedral site as shown in Fig. 4B but rather a position close to a tetrahedral site. This is an indication that these versions of ReaxFF may not be able to reproduce proper carbon behavior in the subsurface.

3.4 Minimum energy path for carbon diffusion in bulk Fe We now turn to the behavior of carbon in bulk Fe. The formation energies of a carbon atom at the octahedral and tetrahedral sites are shown in Table 5. EAM predicts that the carbon atom prefers to be located at the octahedral site. This is in agreement with experiments [47, 48] and DFT calculations [49, 50]. As is mentioned in

Table 4 Carbon adsorption energies on a Fe(110) surface relative to the most stable configuration (LB).

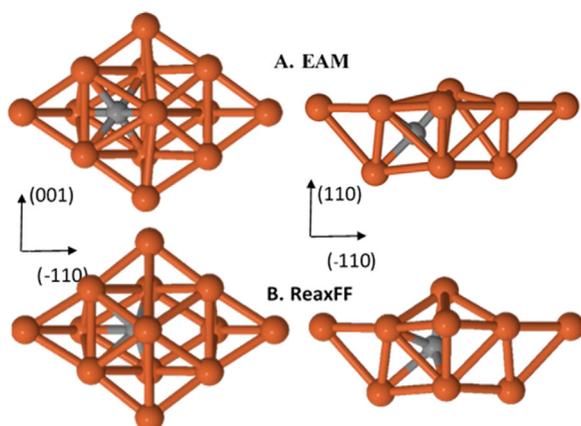|	SB	OT	TF
ΔE (eV) DFT	1.08	1.54	0.03
ΔE (eV) EAM	0.62	1.41	0.05
ΔE (eV) ReaxFF-1	1.33	4.21	0.88
ΔE (eV) ReaxFF-2	1.41	2.75	1.60

Figure 4 Most stable structure for a carbon atom in the Fe(110) subsurface calculated using the EAM (A) and using the the ReaxFF (B). Brown: Fe atoms, grey: carbon atom. Fe–Fe (brown) and Fe–C (brown–grey) bonds are also shown.
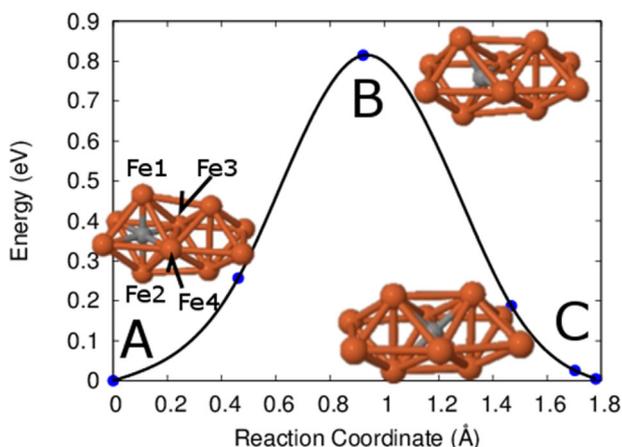

Figure 5 Minimum energy path of carbon diffusion in bulk Fe calculated by using the NEB method with the EAM potential. The C atom moves from one octahedral site (A) to the nearest octahedral site (C) via a tetrahedral site (B). The discrete data points are connected by a smoothing line. Brown: Fe atom, grey: carbon atom. Equivalent calculations using DFT have been carried out by several researchers [50] including the developers of the EAM potential [38] and served as an important benchmark for the fitting of the potential.

the introduction, the ReaxFF potential is expected to be more appropriate for studying surface properties. However, in this paper we show that this assumption does not hold for C environments. According to our calculations, as shown in Table 5, both versions of the ReaxFF potential incorrectly predict the tetrahedral site as the most stable interstitial site for carbon in bulk Fe. Therefore, none of the ReaxFF versions are suitable to study the behavior of carbon in bulk Fe. This is why migration calculations presented below will focus on the EAM forcefield.

Figure 5 depicts the minimum energy path of carbon diffusion in bulk Fe calculated using the NEB method with the EAM potential. The octahedral site was used as the initial position of carbon in bulk Fe as it is the preference position as shown in Table 5. In this plot, the discrete data points are connected by a smooth line. This value is also in good agreement with the DFT result of 0.86 eV [50] and the experimental migration energy of carbon which lies between 0.81 and 0.83 eV [51]. Our NEB calculation also shows that carbon moves from one octahedral site (A) to the nearest octahedral site (C) via a tetrahedral site (B), as shown in Fig. 5. The geometries of carbon at minimum-1 (A), at saddle point (B) and at minimum-2 (C) are given in Table 6. These are in agreement with the DFT calculations [50].

3.5 Minimum energy path for carbon diffusion from surface to subsurface We now turn to carbon diffusion into the subsurface using the already identified preferential sites as initial and final positions. The initial

carbon position on the surface obtained by the EAM is further above the surface (0.782 Å) than by DFT calculations (0.327 Å), yet, the final position is in a good agreement with our DFT calculation. The EAM minimum energy path for carbon diffusion from Fe(110) surface to subsurface is similar to that of DFT. However, it has a longer reaction path than the DFT path, a result of the C–Fe bond lengths on surface being overestimated by the EAM, combined with the collective contribution from a slightly larger lattice parameter. The potential was fitted against the Fe–C bulk systems and does not reproduce exactly the local structure of the Fe–C complex in the vicinity of the surface, especially when the C atom is adsorbed on the surface. The local environment of the C atom is completely different from that in a bulk and therefore, the adsorption sites feature slightly different structures, mainly, in terms of Fe–C bond distances. However, we show that despite the fact that the potential was not fitted with surface data, it yields results in good agreement with DFT. The order of preference for adsorption sites is preserved and the qualitative aspects of the carbon minimum-energy path from surface to subsurface, as shown in Fig. 6, is similar to that obtained with DFT calculations. In Fig. 6, the reaction coordinate of the DFT is shifted so that its initial image will be at the same coordinate as an EAM's image denoted with "A" (image A). Image A is an image, which has a carbon distance from surface close to the distance found in the initial image of the DFT. The carbon atom moves only vertically down toward the surface from the initial image to the image A in the EAM calculations. Figure 7 shows the shifted minimum energy path of the EAM if image A in Fig. 6 is set as a new initial image.

Table 5 Carbon formation energies at interstitial configurations.

energy (eV)	EAM	DFT [49]	ReaxFF-1	ReaxFF-2
octahedral site	−10.04	−10.71	−6.27	−5.83
tetrahedral site	−9.23	−9.787	−7.49	−6.56
difference	0.81	0.923	1.22	0.73

Original

Paper

Phys. Status Solidi B 254, No. 2 (2017)

(7 of 10) 1600408

Table 6 Bond lengths of the minimum and saddle point configurations.

configuration	EAM			DFT [50]		
	Fe1-Fe2 (Å)	Fe3-Fe4 (Å)	C-Fe4 (Å)	Fe1-Fe2 (Å)	Fe3-Fe4 (Å)	C-Fe4 (Å)
minimum 1	3.57	2.79	1.98	3.559	2.797	1.978
saddle point	3.21	3.21	1.79	3.361	3.353	1.820
minimum 2	2.79	3.57	1.79	2.811	3.550	1.775

The energy barrier predicted using the NEB with EAM for carbon atom diffusion from LB site on surface to subsurface is 1.03 eV and from subsurface to surface is 0.66 eV. This is in agreement with our DFT calculations (0.98 and 0.45 eV for surface to subsurface and vice-versa, respectively) and those from the literature (1.18 and 0.56 eV for surface to subsurface and vice-versa, respectively) [46].

These results show that, although the EAM was not developed for surface properties, it can produce reasonable carbon diffusion behavior from surface to subsurface.

3.6 Minimum energy path for carbon migration on surface As discussed, Fig. 8 shows the minimum energy path for carbon migration on the Fe(110) surface calculated using the NEB method with both EAM potential and DFT. The migration of C was not attempted with the ReaxFF potentials as the intermediate images always relaxes back to the initial configuration − LB site, as presented previously, rendering the NEB pathway extremely difficult to converge. For EAM, the energy barrier for carbon to move from a LB site to the nearest LB site is 0.62 eV while for the DFT it is 1.08 eV. As the DFT predicts a slightly smaller lattice parameter than the EAM (2.83 Å compared to 2.85 Å) it has a shorter reaction path compared to the EAM. The path of the carbon migration predicted using the NEB method by the EAM and the DFT is

illustrated in Fig. 9. From the minimum-energy state at the LB site, the carbon atom first moves to the TF site and then to the transition state at the SB site. From SB, it jumps to the neighboring TF site and finally proceeds to the neighboring LB site. The migration path also shows that the SB site is the saddle point and there are local minima at TF sites.

However, according to the DFT, the SB site (transition state) has a much higher energy (1.08 eV) with respect to the LB site (minimum-energy state) than what is found with the EAM (0.62 eV). Furthermore, DFT does not predict a local minimum at the TF sites. The energy of the system rises slowly from the minimum-energy state (LB) to the TF site and then sharply rises as the C atom moves to the SB site (transition state). There is an important qualitative difference between the description of the migration mechanism by DFT and the EAM. As the EAM features a much lower carbon migration barrier on the surface (0.62 eV) in comparison to the surface-to-subsurface diffusion barrier (1.03 eV, see Section 3.5), once a carbon atom is on the surface, it will rather migrate on the surface than diffuse into subsurface. The DFT, on the other hand, predicts that the two barriers are comparable, with the surface-to-subsurface barrier being slightly lower (0.98 eV, see Section 3.5). Table 7 presents the comparison of the bond lengths for the migration of carbon on the surface predicted by the EAM and the DFT. The trends are similar and, overall the results again show that although the EAM was not developed
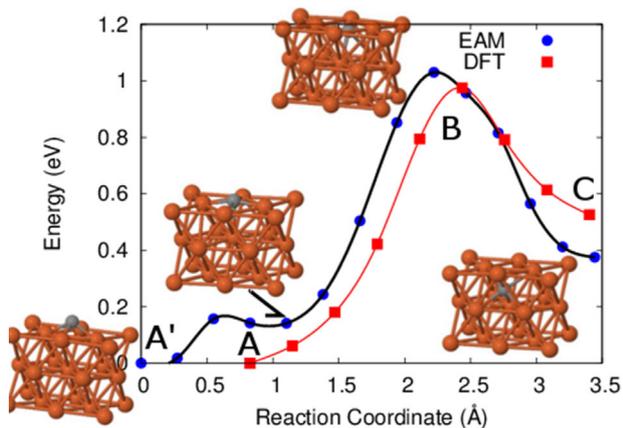

Figure 6 Minimum energy path of carbon diffusion through Fe(110) surface into subsurface calculated by using the NEB method with the EAM potential and the DFT. The reaction coordinate of the DFT is shifted so that its initial image is located at the same coordinate as image A of the EAM.
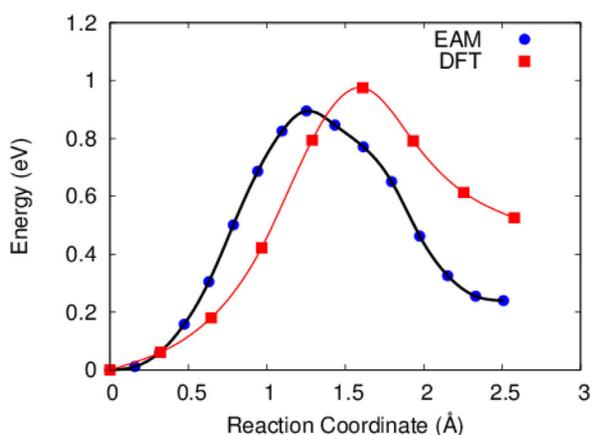

Figure 7 Minimum energy path of carbon diffusion through Fe(110) surface into subsurface. Here, image A of the EAM in Fig. 7 is set as a new initial image.
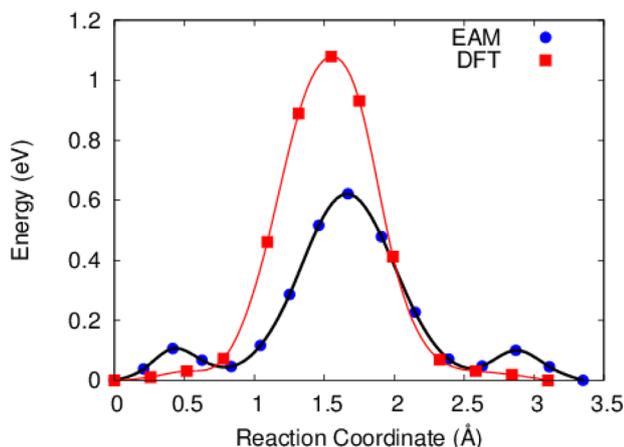
Figure 8 Minimum energy path of carbon diffusion over the Fe(110) surface calculated using the NEB method with the EAM potential and DFT.
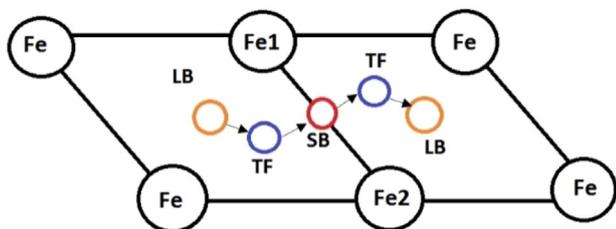

Figure 9 Migration path of carbon on the Fe(110) surface predicted by the NEB method using the EAM and DFT. The C atom migrates between LB sites (yellow circle) by crossing a barrier at the SB site (red circle) and local minima at the TF sites (blue circle) on the way.

especially for surface properties, its predictions regarding the behavior of carbon on the (110) Fe surface are reasonable.

4 Applying the EAM potential Once we have identified the EAM potential as providing the best agreement with DFT calculation, we apply it to characterize C diffusion in Fe in the presence of a surface. As barriers are high, molecular dynamics is not appropriate for this type of calculations and we turn rather to the kinetic activation–relaxation technique (k-ART), a method designed to explore

energy landscapes of complex atomistic systems, which makes it possible to study kinetics in longer time scales, as discussed in the Computational Method's section. As a demonstration, we compare the diffusion coefficients of C in the bulk and on the (110) surface. As ReaxFF does not predict correctly the migration path of C in the bulk, we only use the EAM potential for this study.

4.1 Carbon diffusion from bulk to surface Diffusion of C from the surface to the bulk is difficult to observe because the energy cost of moving into the bulk. To speed up the calculations, we investigate the reverse trajectory, that is, diffusion from the bulk to the surface. The energy landscape produced during this simulation can then be easily used to understand the reverse process.

The C atom is initially located into the bulk and left to find its path to the surface. The surface to the bulk diffusion barriers can then be obtained by simply reversing the trajectory in the KMC and checking the reverse barriers.

As the carbon atom comes near the surface, k-ART automatically captures elastic effects, changing the bulk diffusion barrier by up to 0.03 eV. These distortions can be seen at around 33 μs in Fig. 10 (top), as it is around this time that the carbon arrives to the surface. The barrier for diffusion from the bulk to the surface is 0.66 eV (KMC step 691–692 in Fig. 10-bottom) and the reverse barrier is ∼1 eV for diffusion from surface to bulk. Now, for C to go beyond the first layer − that is, to move back from step 693 to step 691 or beyond – it must cross an affective barrier of ∼1.2 eV, as this is the maximum hill of the energy land scape respect to the ground state, which is when C is on the surface (step 693).

4.2 Carbon migration on the Fe(110) surface Once the carbon atom arrives on the Fe(110) surface, the minimum energy falls to the lowest energy state, ∼0.4 eV below the octahedral site in the bulk. It then crosses small barriers of ∼0.1 eV to hop to states 0.04 eV higher than the most stable configuration, as shown in the bottom panel of Fig. 10 (KMC step 693–694). This is due to the back and forth hopping between the LB and TF sites which are close neighbors. The migration between two LB sites takes place on a longer time scale and is shown in the bottom panel of Fig. 10. The top panel shows that when carbon is already on the surface (around 33 μs) it diffuses by crossing

Table 7 Bond lengths for the migration of C on the surface. All bond lengths are given in Å.

configuration	EAM			DFT		
	C–Fe1	C–Fe2	Fe1–Fe2	C–Fe1	C–Fe2	Fe1–Fe2
LB (minimum)	1.74	2.02	2.4	1.798	1.951	2.598
TF	1.78	1.73	2.46	1.812	1.833	2.608
SB (saddle)	1.66	1.66	2.46	1.745	1.745	2.746

Original
Paper

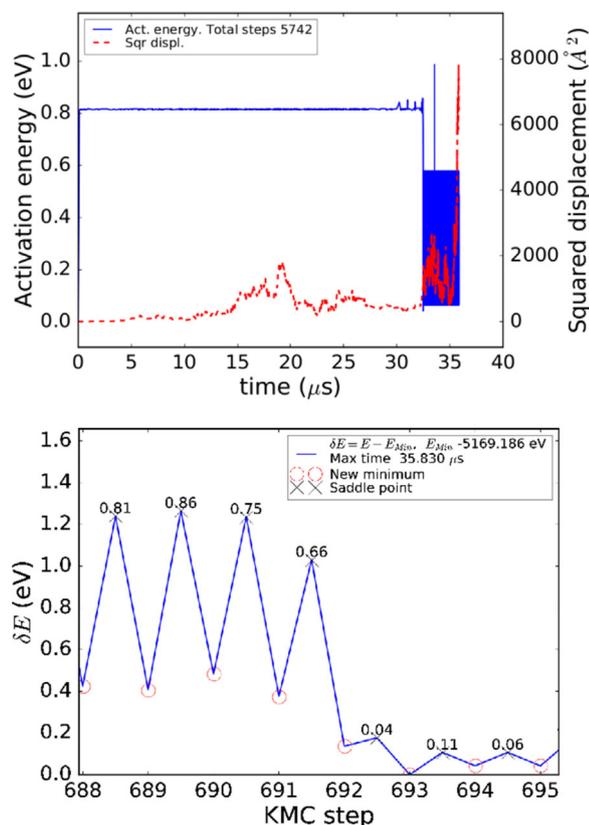Phys. Status Solidi B 254, No. 2 (2017)   (9 of 10) 1600408

Figure 10 Barrier energy and square displacement for carbon diffusion from bulk to surface predicted by k-ART at 600 K, as a function of time (top). A close-up view of the energy profile is shown with respect to the KMC steps as the carbon atom emerges from the bulk onto the surface (bottom).

a barrier of 0.58 eV, as predicted in Section 3.6. Following other KMC simulations, we use a fixed prefactor of $10^{13}\,\mathrm{s}^{-1}$ associated with the Debye frequency [34]. With it, the k-ART simulations predict a diffusion coefficient on the surface of $7.8 \times 10^{-13}\,\mathrm{m}^2\,\mathrm{s}^{-1}$ at 600 K. Therefore, according to the EAM potential, carbon migration on the Fe(110) surface is approximately one order of magnitude faster than in the bulk at this temperature.

5 Conclusions Molecular statics and kinetic Monte-Carlo studies of carbon adsorption, absorption, and diffusion on the Fe(110) surface were used to compare empirical potentials and validate their predictions against DFT. Although the EAM potential used here was initially developed for ferritic Fe–C bulk systems, we show that it predicts reasonably reliable surface properties of Fe. More precisely, EAM predicts the long-bridge site as the preferred location for carbon on the Fe(110) surface and the octahedral site in the Fe subsurface. This is in good agreement with the DFT calculations. The ReaxFF predicts reasonably good surface properties for Fe and carbon on Fe surface. However, it is not able to predict properly carbon behavior in the Fe subsurface and at interstitial sites in the

bulk. The diffusion of C on and into the Fe(110) surface were studied using the NEB method. The energy barrier for surface-to-subsurface diffusion is 1.03 eV which is close to the DFT prediction of 0.98 eV. The energy barrier of carbon diffusion in bulk Fe is 0.8145 eV which is also comparable to the DFT results and in a good agreement with experimental migration energy data. In bulk, EAM indicates that carbon diffuses from one octahedral site to the next octahedral site via a tetrahedral site, in agreement with the existing models. EAM predicts that a carbon atom on the surface migrates from one LB adsorption site to another, via a SB site, with a barrier of 0.62 eV. Therefore, according to EAM, once a C atom is on a Fe(110) surface, it will migrate on the surface instead of diffusing into subsurface. On the other hand, the DFT calculations predict a higher energy for the SB site, 1.08 eV, as a higher migration barrier. As the energy barrier for surface to subsurface diffusion is slightly lower, according to DFT, C is more likely to diffuse into subsurface, than on the surface. We also apply EAM in k-ART to compare diffusion properties. We find that the diffusion coefficient on the Fe(110) surface is one order of magnitude lower than in bulk.

In summary, the ReaxFF force field is better suited for reaction of surfaces and less suited for subsurface and bulk diffusion properties. The EAM potential, on the other hand, seems reasonable for surface properties although underestimating the surface diffusion barrier with respect to DFT but it can be trusted for subsurface and bulk properties.

These results demonstrate that it is essential to fully characterize empirical potentials when moving to study complex set-ups as no such forcefield can describe both surface and subsurface/bulk environments, correctly. This is why we suggest the use of a hybrid approach using the EAM potential conjunction with ReaxFF potential to tackle the complex problem of carburization and metal dusting. Following on the methodology proposed recently in Ref. [13], surface and gas reactions on surfaces would be handled with ReaxFF then EAM could be used to study subsurface and bulk diffusion properties, opening up the possibility of performed large-scale reliable simulations of this and other similar heterogenous reactions.

References

[1] D. Young, J. Zhang, C. Geers, and M. Schütze, Mater. Corrosion **62**(1), 7–28 (2011).
[2] M. Daw and M. Baskes, Phys. Rev. B **29**(12), 6443–6453 (1984).

[3] C. S. Becquart, J. M. Raulot, G. Bencteux, C. Domain, M. Perez, S. Garruchet, and H. Nguyen, Comput. Mater. Sci. **40**(1), 119–129 (2007).

[4] R. Veiga, C. S. Becquart, and M. Perez, Comput. Mater. Sci. **82**, 118–121 (2014).

[5] E. Clouet, S. Garruchet, H. Nguyen, M. Perez, and C. S. Becquart, Acta Mater. **56**, 3450–3460 (2008).

[6] R. G. A. Veiga, M. Perez, C. S. Becquart, E. Clouet, and C. Domain, Acta Mater. **59**, 6963 (2011).

[7] R. Veiga, H. Goldenstein, M. Perez, and C. Becquart, Scr. Mater. **108**, 19–22 (2015).

[8] O. A. Restrepo, N. Mousseau, F. El-Mellouhi, O. Bouhali, M. Trochet, and C. S. Becquart, Comput. Mater. Sci. A **112**, 96–106 (2016).

[9] S. Garruchet and M. Perez, Comput. Mater. Sci. **43**(2), 286–292 (2008).

[10] N. Gunkelmann, H. Ledbetter, and H. M. Urbassek, Acta Mater. **60**(12), 4901–4907 (2012).

[11] C. Sinclair, M. Perez, R. Veiga, and A. Weck, Phys. Rev B **81**, 224204 (2010).

[12] C. Zou and A. van Duin, JOM **64**(12), 1426–1437 (2012).

[13] M. Islam, C. Zou, A. van Duin, and S. Raman, Phys. Chem. Chem. Phys **18**, 761 (2016).

[14] A. C. T. van Duin, S. Dasgupta, F. Lorant, and W. A. Goddard III, J. Phys. Chem. A **105**(41), 9396–9409 (2001).

[15] G. Kresse and J. Hafner, Phys. Rev. B **48**, 13115 (1993).

[16] G. Kresse and J. Furthmuller, Comput. Mater. Sci. **54**(11), 169 (1996).

[17] G. Kresse and J. Furthmüller, Phys. Rev. B **54**, 169 (1996).

[18] A. Chakrabarty, O. Bouhali, N. Mousseau, C. S. Becquart, and F. El-Mellouhi, J. Appl. Phys. **120**, 055301 (2016).

[19] S. Plimpton, J. Comput. Phys. **117**(1), 1–19 (1995).

[20] G. Henkelman, B. P. Uberuaga, and H. Jonsson, J. Chem. Phys. **113**(22), 9901–9904 (2000).

[21] G. Henkelman and H. Jonsson, J. Chem. Phys. **113**(22), 9978–9985 (2000).

[22] A. Nakano, Comput. Phys. Commun. **178**(4), 280–289 (2008).

[23] D. Sheppard, R. Terrell, and G. Henkelman, J. Chem. Phys. **128**(13), 134106 (2008).

[24] F. El-Mellouhi, N. Mousseau, and L. J. Lewis, Phys. Rev. B **78**, 153202 (2008).

[25] G. Barkema and N. Mousseau, Phys. Rev. Lett. **77**, 4358 (1996).

[26] R. Malek and N. Mousseau, Phys. Rev. E **62**, 7723 (2000).

[27] E. Machado-Charry, L. K. Béland, D. Caliste, L. Genovese, T. Deutsch, N. Mousseau, and P. Pochet, J. Chem. Phys. **135**, 034102 (2011).

[28] B. McKay, Congressus Numerantium **30**, 45–87 (1981).

[29] B. McKay and A. Piperno, J. Symb. Comput. **60**, 94–112 (2014).

[30] A. Bortz, M. Kalos, and J. Lebowitz, J. Comput. Phys. **17**(1), 10–18 (1975).

[31] A. Voter, Phys. Rev. B **34**, 6819 (1986).

[32] D. J. Young and J. Zhang, ECS Trans. **16**(44), 3–15 (2009).

[33] A. Wiltner, Ch. Linsmeier, and T. Jacob, J. Chem. Phys. **129**, 084704 (2008).

[34] L. K. Béland, P. Brommer, F. El-Mellouhi, J. Joly, and N. Mousseau, Phys. Rev. E **84**, 046704 (2011).

[35] N. Mousseau, L. Béland, P. Brommer, F. El-Mellouhi, J. Joly, G. N'Tsouaglo, O. Restrepo, and M. Trochet, Comput. Mater. Sci. B **100**, 111–123 (2015).

[36] M. Acet, H. Zahres, E. Wassermann, and W. Pepperhoff, Phys. Rev. B **49**, 6012 (1994).

[37] F. Stern, Phys. Rev. **116**(6), 1399–1417 (1959).

[38] C. Domain and C. Becquart, Phys. Rev. B **65**(2), 024103 (2001).

[39] P. A. Korzhavyi, I. A. Abrikosov, B. Johansson, A. V. Ruban, and H. L. Skriver, Phys. Rev. B **59**(18), 116693–111703 (1999).

[40] S. Kim and W. Buyers, J. Phys. F **8**(5), L103 (1978).

[41] J. J. Adams, D. S. Agosta, R. G. Leisure, and H. Ledbetter, J. Appl. Phys. **100**(11), 113530 (2006).

[42] G. J. Ackland, M. I. Mendelev, D. J. Srolovitz, S. Han, and A.V. Barashev, J. Phys.: Condens. Matter **16**(27), S2629 (2004).

[43] W. Tyson and W. Miller, Surf. Sci. **62**(1), 267–276 (1977).

[44] C. Xu and D. O'Connor, Nucl. Instrum. Methods Phys. Res. B **53**(3), 315–325 (1991).

[45] H. D. Shih, F. Jona, U. Bardi, and P. M. Marcus, J. Phys. C: Solid State Phys. **13**(19), 3801 (1980).

[46] D. Jiang and E. Carter, Phys. Rev. B **71**(4), 045402 (2005).

[47] G. Williamson and R. Smallmann, Acta Crystallogr. **6**, 361 (1953).

[48] D. Jack and K. Jack, Mater. Sci. Eng. **11**, 1 (1973).

[49] C. Domain, C. Becquart, and J. Foct, Phys. Rev. B **69**, 144112 (2004).

[50] D. E. Jiang and E. A. Carter, Phys. Rev. B **67**, 214103 (2003).

[51] A. Le Claire, in: Numerical Data and Functional Relationships in Science and Technology, edited by H. Mehrer (Springer-Verlag, Berlin, 1990), pp. 480–481.